Wiktor Wciślik
Structure and Environment 2024, vol. 16, (2), pp. 97-110, Article number: el 009
https://doi.org/10.30540/sae-2024-009

Structure and Environment
ISSN 2081-1500
e-ISSN 2657-6902
https://content.sciendo.com/sae
https://sae.tu.kielce.pl

sciendo

Kielce University of Technology

DOI: 10.30540/sae-2024-009

SELECTED MICROSTRUCTURAL PHENOMENA IN FSW JOINTS

WYBRANE ZAGADNIENIA MIKROSTRUKTURY SPOIN WYKONANYCH W TECHNOLOGII FSW

Wiktor Wciślik
Kielce University of Technology, Poland

Abstract

The article is a literature review on selected phenomena leading to microstructural changes in material welded using the friction stir welding (FSW) method. Particular attention was paid to the phenomena of grains recrystallization, as well as dissolution and reprecipitation of second phase particles, resulting from temperature changes during FSW. Temperature transformations in different zones of the FSW joints were characterized. The role of base material phase transformation in the formation of new particles is discussed. In the tested aluminum alloys and stainless steels, this process was particularly intensified in the heat affected zone (HAZ). In areas subjected to high temperature and significant plastic deformation (nugget zone and thermomechanically affected zone), this phenomenon did not occur or was characterized by small intensity. It was indicated that the phenomenon of particle formation clearly affects the strength parameters of the joint.

Keywords: Friction Stir Welding (FSW), microstructure, grain, recrystallization, precipitation, strengthening particle

Streszczenie

W artykule przedstawiono przegląd literatury dotyczący wybranych zjawisk prowadzących do zmian mikrostrukturalnych w metalach spawanych metodą zgrzewania tarciowego (FSW). Szczególną uwagę zwrócono na zjawiska rekrystalizacji ziaren oraz rozpuszczania i ponownego wytrącania cząstek drugiej fazy, zachodzące jako efekt zmian temperatury podczas FSW. Scharakteryzowano zmiany temperatury w różnych strefach złączy FSW. Omówiono rolę przemian fazowych materiału podstawowego w powstawaniu nowych cząstek. W badanych stopach aluminium i stalach nierdzewnych proces ten był szczególnie nasilony w strefie wpływu ciepła (SWC). W obszarach narażonych na działanie wysokiej temperatury i znacznych odkształceń plastycznych (jądro zgrzeiny i strefa uplastycznienia termomechanicznego) zjawisko to nie występowało lub charakteryzowało się niewielkim natężeniem. Wykazano, że zjawisko tworzenia cząstek wyraźnie wpływa na parametry wytrzymałościowe złącza.

Słowa kluczowe: zgrzewanie tarciowe (FSW), mikrostruktura, ziarno, rekrystalizacja, wydzielenie, utwardzanie wydzieleniowe

1. INTRODUCTION

Friction stir welding (FSW) is described in the literature as a modern welding technique, although its history dates back over 30 years. Originally developed for aluminum and other soft metals, it has been greatly developed in recent years [1] and is also used for various metals (magnesium, titanium, copper, nickel, steel), polymers [2] and others, including dissimilar components [3]. Ease of use, simplicity and universality result in its wide application in the industry, primarily in the automotive, civil engineering, aviation, shipbuilding, chemical and others.

FSW involves introducing a non-consumable tool between the edges of the welded elements and its

*Kielce University of Technology, Poland, e-mail: wwcislik@tu.kielce.pl

uniform movement. The tool consists of a shoulder, whose main task is to generate heat and soften the material, and a pin, intermixing the materials and leading to a permanent joining of both elements. Importantly, during FSW there is no material melting, therefore it is a solid state process. The schematic diagram of FSW is presented in Figure 1.

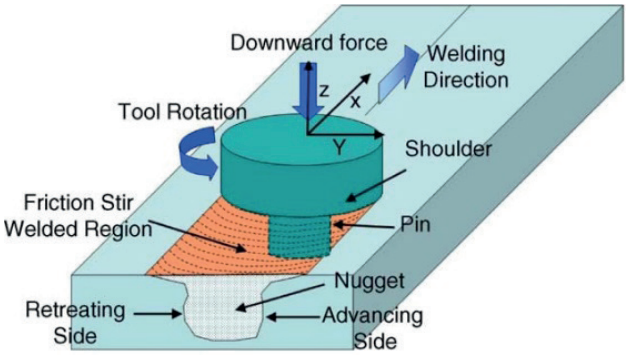

Fig. 1. Scheme of FSW technology [4]

Compared to traditional welding methods, FSW has many advantages that can be divided into 3 basic groups [4]:

1. Metallurgical – slight deformation of welded elements, repeatability and dimensional stability, high metallurgical quality of the joint, no cracking, no loss of alloying elements, fine microstructure.
2. Environmental – no need for special preparation of the welded surfaces and the use of protective gases, no need for additional consumable materials.
3. Energetic – low energy consumption, low structure weight.

The great advantage of FSW is its versatility and the ability to make various types of joints (Fig. 2).

In recent years, FSW technology has undergone tremendous development. This applies primarily to the patenting of various types of tools and additional material processing, which can be classified as new subtypes of FSW. Technologies derived from typical FSW are used not only for welding elements, but also for modifying the surface properties of a single element, repairing material defects etc.

For instance, Friction Stir Processing (FSP) is a technology derived from FSW. As in FSW, a rotating tool (pin and shoulder) is used, but not for welding elements, but for surface material modification of a single workpiece [6, 7]. FSP is a modern technology for the production of ultra-fine grain (UFG) materials. The effectiveness of FSP depends on the type of material in the delivery state, primarily on its microstructure and chemical composition.

Another technique based on FSW is Friction Stir Alloying (FSA), which, similarly to FSP, involves modification of material properties, but with the addition of a consumable material. As a result, a composite is formed, consisting of the basic (modified) material and the second phase dispersed in it. In practice, due to the difficulty of dispersing the filler uniformly in the volume of the base material, usually the material modification covers only its thin near-surface layer, which, however, significantly improves such properties as hardness or corrosion resistance [8].

An extensive and detailed description of technologies derived from FSW can be found in [9].

The present article discusses selected issues related to microstructural changes occurring in material during FSW/FSP, with particular emphasis on steel and aluminum alloys. Chapter 2 describes

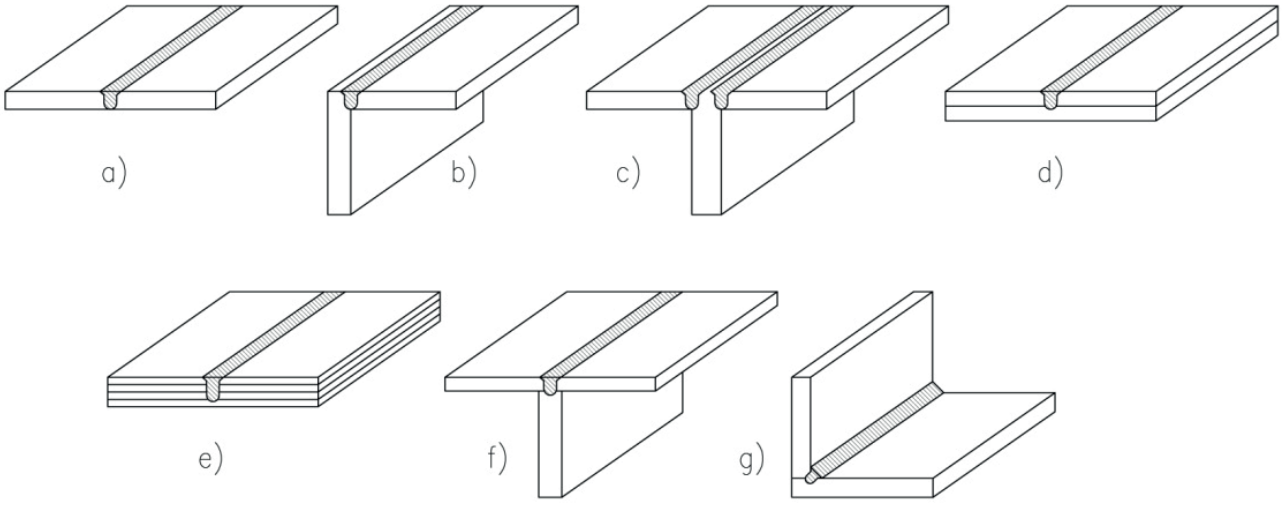

Fig. 2. Different types of FSW joints: a) square butt; b) edge butt; c) T butt joint; d) lap joint; e) multiple lap joint; f) T lap joint; g) fillet joint, based on [4, 5]

the FSW joint zones in which, due to the different thermomechanical history, various processes occur. The issues of recrystallization (Chapter 4) and the phenomena related to the reinforcing particles (primarily dissolution, reprecipitation and coarsening) are discussed (Chapter 5). Considering that these issues are closely related to temperature changes, in Chapter 3 a brief description of thermal phenomena in FSW/FSP is provided.

This article focuses on microstructural transformations during FSW, but its scope does not include the characteristics of thermomechanical processes occurring during welding, as well as unsteady heat flow and phase transformations. These issues are discussed, for example, in [10-12]. The influence of welding parameters on the physical and strength properties of joints is discussed, for example, in [13].

The results of experimental studies and observations of the material microstructure are described. The wide range of analytical and numerical models, which in recent years have contributed to a better understanding of the physical phenomena occurring during FSW/FSP, is not discussed. A comprehensive review can be found in [5, 14].

2. OVERVIEW

Depending on the position with respect to the tool, the material experiences various types of thermomechanical transformations that determine its subsequent microstructure and, consequently, also its strength properties. For this reason a typical FSW joint cross section consists of nugget zone (NZ, or stirred zone – SZ), thermomechanically affected zone (TMAZ) and heat affected zone (HAZ, Fig. 3).

The joining of elements takes place in NZ. This is the zone of direct impact of the tool pin and therefore experiences significant deformation and high temperature. For this reason, recrystallization and formation of fine, equalized grains occur in NZ. The TMAZ, on the other hand, can be defined as a transition zone in which the deformation is smaller and complete recrystallization does not occur. No plastic deformation is observed in HAZ, so its microstructure (except for strengthening particles) is very similar to the base material. The size of each of these zones depends on the type of material, tool and welding technological parameters [16].

The quality and parameters of the entire joint depend on the microstructure of each of these zones. To assess the quality of joints made with the FSW technique, transmission electron microscopy (TEM), optical microscopy and X-ray diffraction are most often used [5].

In turn, to understand the formation and properties of FSW joints, it is crucial to determine the flow of material during welding. For this purpose, various flow visualization techniques are used, such as placing a marker (contrast material) [17-20], or combining different alloys [21, 22]. It should be borne in mind that the flow of material is highly dependent on the shape of the tool [4].

3. EFFECT OF TEMPERATURE

In the FSW process material experiences both significant plastic deformation and high temperature. In the first phase of inserting the tool, heat is generated primarily by friction at the contact point between the pin and the welded material. Already during the welding itself (after the tool is fully inserted), heat is generated primarily by friction at the contact surface between the shoulder and the welded material. A certain amount of heat is also the result of the material deformation [23]. Higher rotational speed of the tool results in higher temperature generation, which in turn translates into better mixing of the

Fig. 3. Typical cross section of a FSW joint [15]

material. The intensity of heating is also related to the type of tool. In addition, the preheating of the workpiece results in local material softening, reduction in the friction coefficient and the associated reduction in heat generation [24]. On the other hand, the change in travel speed does not significantly affect the peak temperature [25, 26].

Depending on the thermal conductivity of the welded material, peak temperature asymmetry between the advancing side (on which the direction of rotation and movement of the tool are consistent) and retreating side can be observed. For example, as observed in [27], the temperature of the 304L stainless steel on the advancing side was about 100K higher. However, such a large scale of this phenomenon occurs quite rarely. The authors attributed this significant difference to the low, compared to other FSW joined materials, thermal conductivity of the tested alloy.

In the stirred zone (SZ) the temperature oscillates around 0.75-0.9T_m (T_m – melting temperature) [28]. In the thermo-mechanically affected zone (TMAZ), the temperature was estimated at 0.6-0.7T_m [29, 30].

Additionally, in some cases (materials characterized by high melting temperature), the heat generated by friction in FSW is not sufficient to soften and thoroughly mix the material, which makes it necessary to provide additional heat from an external source.

On the other hand joint cooling can be also used (especially for soft materials) to prevent excessive growth of recrystallized grains and dissolution of reinforcing particles [4, 26].

In general, the temperature distribution depends on the type of tool used and technological parameters, namely:

- Heat is generated primarily by the shoulder – it is commonly believed that the shoulder produces about 80% of the heat released [31, 32].
- With constant tool travel speed, the maximum temperature increases as the rotation speed increases.
- The maximum temperature increases with the increase of rotation speed/travel speed ratio [4].

The above mentioned thermal effects, regardless of plastic deformation, cause changes in the microstructure of the welded material (grain size and boundaries, dissolution and coarsening of the second phase particles, change in texture, etc.). Thus, temperature measurement can be used as an auxiliary tool that allows for an indirect assessment of the joint quality [33].

To understand these relationships, it is important to measure the temperature distribution in the weld area and its surroundings. Measuring the temperature of the material, due to its plastic deformation, is technically difficult. The use of a thermal imaging camera, although not problematic, does not provide insight into the interior of the material. Due to the impossibility of placing the measuring instruments directly in the welding zone, measurements are made in its vicinity, then the obtained results are extrapolated [14, 34]. One of the measurement possibilities is to embed a thermocouple in the welded material in the vicinity of the tool [4]. High measurement accuracy is obtained when thermocouples are embedded in several holes of different depths [35]. Moreover, thermocouples embedded inside the tool, as well as tool-workpiece thermocouple (measurement based on thermoelectric effect between tool and workpiece) are used [14]. The temperature distribution can be also assessed indirectly, based on the analysis of the weld microstructure.

Regardless of measurements and observations, many thermomechanical models combining friction and plastic deformation with thermal effects have been developed. As already mentioned, modeling issues is beyond the scope of this paper. A comprehensive review of the thermomechanical models related to FSW/FSP can be found, for example, in [24].

4. GRAIN RECRYSTALLIZATION AND REFINEMENT

As a result of plastic deformation, grain size is reduced [36, 37], which, according to the Hall-Petch relationship, directly translates into an increase in the material strength. Grain refinement occurs first of all by dynamic recrystallization, which is the dominant mechanism in SZ and TMAZ. Especially in the SZ fine, equiaxed recrystallized grains are observed. Three basic submechanisms can be distinguished [38, 39]:

- Discontinuous dynamic recrystallization (DDRX) – nucleation and growth of new grains, characteristic for materials of low and medium stacking fault energy (SFA).
- Continuous dynamic recrystallization (CDRX) – formation of low angle boundaries, gradual increase in boundary misorientation and continuous accumulation of the dislocations introduced by plastic deformation.
- Geometric dynamic recrystallization (GDRX) – grain refinement occurs through a process of grain elongation and thinning leading to an increase in grain boundary area [40].

The dynamic recrystallization mechanism that occurs in the material during FSW/FSP depends on temperature and strain. DDRX occurs at high temperature and low strain while CDRX occurs at medium temperature and high strain [41, 42].

Due to the fact that after passing the FSW/FSP tool, material is subjected to high temperature for some time, especially in the nugget zone, one more recrystallization mechanism is observed, namely metadynamic recrystallization (MDRX). MDRX results from the post deformation annealing in the SZ [41].

The homogeneity of the microstructure increases with increasing temperature and decreasing strain rate. In practice, a homogeneous structure is formed in SZ, while partial recrystallization is observed in TMAZ [43].

Another mechanism is static recrystallization, which involves the nucleation of new, undeformed grains and their subsequent growth. Material recrystallized in this way gradually replaces the microstructure of the parent material. The recrystallized and non-recrystallized areas are clearly separated.

Static recrystallization can also be divided into two separate submechanisms, namely discontinuous static recrystallization (DSRX) and continuous static recrystallization (CSRX). DSRX is characteristic of low SFE materials and occurs at temperatures above $0.5T_m$. Recrystallization occurs by migration of the high-angle grain boundary (HAGB) existing in material into the deformed matrix in a heterogeneous manner.

For materials with high SFE, static recrystallization most often takes the form of CSRX. In this case, sites of grains nucleation consist partly of high-angle grain boundaries (HAGBs) and low-angle grain boundaries (LAGBs). In terms of CSRX, two additional submechanisms can be distinguished:

- Migration of LAGBs – growth of subgrains in the presence of an orientation gradient resulting from geometrically necessary dislocations.
- Coalescence of neighboring subgrains through the decomposition of a low misorientation LAGB [41, 44].

Important factor affecting grain refinement is the need for efficient and quick heat dissipation [38]. Various liquid cooling systems (water, nitrogen and others) are used for this purpose.

The efficiency of FSW/FSP in grain size reduction and increase in material strength also depend on the shape of the tool. For example, Prabhu et al. [45] demonstrated that in aluminum AA6061-rutile composite the square pin produced finer grains than the cylindrical threaded one.

The effect of the type of tool on the material thermomechanical transformation is particularly clear when using a bobbin tool (BT, 2 shoulders on both sides of the joined workpieces). The amount of heat generated by the friction of two shoulders is greater than in the case of classic tools. In addition, energy dissipation and joint cooling are difficult. This obviously affects the microstructure of the weld and its properties. The impeded heat outflow causes that the grains affected by the both shoulders are larger than in the nugget zone (NZ) [9]. In addition, grains in NZ and HAZ are larger than for single shoulder tools [46]. As discussed in the literature, the use of BT for Al and Mg alloys, due to grain coarsening, results in low strength parameters of the joints.

Another possibility to increase the efficiency of FSW/FSP in grain refinement is the multipass technique. Each time the tool is passed through the material, the grain size gradually decreases.

For some materials, recrystallization is preceded by static recovery, which is associated with a change in the dislocation arrangement. It may result from:

- dislocation annihilation;
- dislocations rearrangement towards lower energy systems;
- subgrains growth [44].

In most pure materials, static recovery occurs at temperatures greater than $0.3T_m$, while recrystallization itself occurs at higher temperatures, above $0.4T_m$. Material ability for static recovery depends on stacking fault energy [41].

The above described microstructural changes occurring during FSW/FSP also result in changes in the mechanism of material failure. Metals used in technology, under normal conditions, crack through nucleation and the development of microvoids. The course of this phenomenon depends to a large extent on the structure of the material, its chemical composition and the presence of foreign phase particles [47-49].

In the case of FSA, grain size reduction and the introduction of an additional material affect the process of voids development. For example, in [50], fracture surfaces of pure (99.9%) aluminum and aluminum-graphene composite, obtained in the FSA process, were compared. The both types of specimens were subjected to tension. Example photographs of fracture surfaces, obtained with the use of transmission electron microscopy (TEM), are shown in Figure 4. Both fractures are ductile in nature, the voids formed as a result of plastic deformation are clearly visible.

However, the significantly smaller diameter of the voids in the composite material is observed.

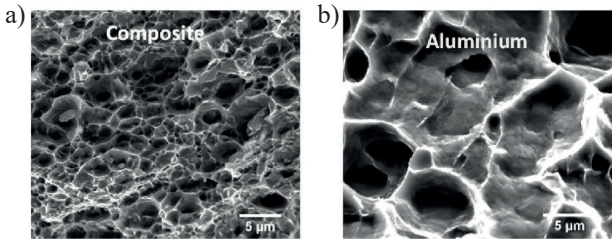

Fig. 4. Fracture surfaces of aluminum-graphene composite made by FSA (a) and pure aluminum (b), [50]

In recent years, many papers have been devoted to the properties of FSW joints made in super duplex (ferritic-austenitic) stainless steels, both in terms of strength properties and microstructure [51]. At the welding temperature of 1300°C, steels of this type change their structure to fully ferritic [52]. Depending on the technological parameters, at lower temperatures, the ferritic-austenitic structure is still observed in the weld zone, but the distribution and morphology of the austenite islands become heterogeneous. On the advancing side, the material experiences the greatest deformation, so that the austenite grains are broken up. As a result, the austenite grains in this area become finer. Moreover, typically for the FSW, grains in the joint area (both ferrite and austenite) are characterized by smaller sizes than in the base material.

The grain size after FSW is also dependent on the technological parameters: the grain size decreases when the tool rotational speed [53, 54] and the rotational speed/travel speed ratio [55] are reduced. This effect is attributed to the lower heat input and its faster dissipation at higher welding speeds.

An example of the analysis of the microstructure and strength parameters of an FSW joint in AISI321 steel is discussed in [56]. The change in the structure and refinement of grains in the stir zone (SZ) was the result of discontinuous dynamic recrystallization (formation and growth of new grains). The course of this phenomenon depended on the welding temperature, which in turn changed with the travel speed of the tool. At the lowest welding speed (25 mm/min), the temperature in SZ reached approximately 80% of the melting temperature of the alloy. The large amount of heat generated resulted in the formation of relatively large grains in the SZ. In the case of a higher welding speed (50 mm/min), the amount of heat supplied was lower (temperature of the order of 67% of the melting temperature) at higher strain rates, which led to a reduction in grain size.

Similar conclusions were drawn from the analysis of the microstructure of FSW joints in 316L stainless steel [57]. Microscopic observations revealed the presence of ultrafine grains in SZ and enlarged reoriented grains in the TMAZ. However, the authors point out that when changing the welding speed, the dominant mechanism influencing the grain size is not the temperature but the strain rate. At higher welding speeds there is less time for dislocation movement and grain boundary relocation, which ultimately results in a reduction in grain size. The dominance of the influence of strain rate over the influence of temperature was also indicated in [58]. The authors of [57] additionally analyzed the weld structure in the TMAZ. In this area, due to the lower temperature than SZ, grain dislocation was the dominant phenomenon. It was further noted that the combination of high tool rotation speeds and low welding speeds resulted in excessive material heating and defect formation.

The authors of [59] analyzed the microstructural changes in SZ in 2205 DSS steel (duplex stainless steel) using quantitative metallography methods. The FSW welding process resulted in a reduction in the ferrite grain size from 8.8 micrometers (in the case of the base material) to 2.71 micrometers. The average austenite grain size decreased from 13.3 micrometers to 2.24 micrometers. At the same time, the authors of [59] emphasize the great importance of the value of the force pressing the tool and its impact on the possibility of making a defect-free joint.

Based on a detailed analysis of the microstructure of 304L austenitic stainless steel, the authors of [60] distinguished 4 stages of the microstructural transformation of the material: compression deformation, rotation deformation, forge and torsion deformation, annealing. In the first phase, LAGB segments are formed in the compression zone, and then partially evolve into HAGBs. Then (the second phase) the coarse grains are transformed into finer ones by DDRX and twinning. In the third phase, after the material is deposited behind the tool, the resulting grains grow and the rotating shoulder introduces forge and torsion deformation. The fourth phase includes the state in which the tool has passed the material and the evolution of the structure is the result of the influence of temperature. Under these conditions, the density of LAGBs decreased and new twin boundaries developed.

5. PRECIPITATION PHENOMENA

5.1. General remarks

Alloys for technical applications are often strengthened by dispersing second phase particles in their structure (e.g. aluminum alloys, metal matrix composites – MMC). It is commonly believed that under the influence of thermomechanical history, the distribution, size and shape of particles changes [61], which directly affects material properties. The particle phase transformation also depends on the chemical composition and temper condition of the base material.

Therefore, a separate problem, relatively often discussed in the literature, is the effect of the temperature and deformation generated during FSW on inclusions and precipitates phenomena [62]. Due to the complex history of thermomechanical changes, depending on the weld zone, pre-existing precipitations are subjected to different processes during FSW. In areas with relatively low temperatures, the existing precipitates coarsen or transform into a more stable phase. In areas with higher temperatures (mainly SZ and TMAZ), the second phase particles dissolve and then reprecipitate. This process depends on the cooling rate, and therefore indirectly also depends on the technological parameters (rapid cooling prevents the formation of new particles). In general, reprecipitation of second phase particles and their growth is often heterogeneous. Depending on the welded material and technological parameters, nucleation and growth of new precipitates is also possible.

Regardless of the stationary processes of reprecipitation, dynamic precipitation (DP) is observed during FSW/FSP, in which particle nucleation and growth are accelerated by plastic deformation. The following mechanisms are possible [63]:

- Particle nucleation acceleration related to the presence of dislocations (heterogeneous nucleation sites).
- Particle growth assisted by pipe diffusion and solute transport by dislocation sweeping.
- Particle coarsening induced by non-equilibrium vacancy concentration.

Particle dissolution is also affected by plastic strain. In general, the mechanism of DP is strongly dependent on temperature, exposure time [64] and plastic strain [65], i.e. variables directly affected by the technological parameters of FSW/FSP. Nowadays deformation induced evolution of second-phase particles is not recognized completely. This refers especially to unstable particles [63].

5.2. Precipitation transformation in steels

Although most of the published works concern the use of FSW for aluminum alloys, the issue of microstructural changes has also been analyzed for various steels.

The paper [66] describes an example of the formation of material discontinuities in the area of the FSW joint of super duplex stainless steel. Particles were not observed neither at the center of the stir zone (SZ) nor at the interface of the SZ and the thermomechanically affected zone (TMAZ). However, microstructural studies showed the presence of a σ-phase in the area of the heat affected zone (HAZ). This phase is defined as the tetragonal intermetallic phase described as Fe-Cr(-Mo). The σ-phase is formed at the boundary of δ-Fe (ferrite) and γ-Fe (austenite) grains. The precipitation of the σ-phase was explained by the effect of heat.

Slightly different conclusions were drawn from the observations of the SZ, primarily on the advancing side. A structure of bright bands was observed at the microscale. The analysis revealed that the bands consist almost entirely of γ-Fe. The δ-Fe phase, which forms the parent material, was not observed in this zone. Moreover, the Cr_2N particles (hexagonal nitride) were also precipitated on the boundaries of γ-Fe grains. Another precipitate was present between the Cr_2N particles (at the triple junction of the γ-Fe grains). As shown by EDX (energy dispersive X-ray spectrometry) analysis, the precipitation was composed of the so called χ-phase ($Fe_{36}Cr_{12}Mo_{10}$).

Moreover, an attempt was made to explain the origin of the observed precipitations. Using the JMatPro software, time-temperature-transformation (TTT) diagrams of the analyzed alloy were developed. It was found that the σ-phase is most intensively formed when the material is exposed to the temperature of 950°C for at least 1 minute. The highest temperature during welding was estimated at about 1100°C, but in the HAZ, where the σ-phase was observed, lower values, of the order of 950°C, should be expected. Based on the simulations, it was also found that precipitation of Cr_2N particles and the χ-phase takes place faster than in the case of the σ-phase.

The authors of [67] studied the influence of tool rotation speed (and thus temperature and strain

rate) on the microstructure of Reduced Activation Ferritic Martensitic (RAFM) steel. Regardless of the rotational speed used (200 or 700RPM), Fe_3C and $M_{23}C_6$ particles were dissolved in SZ and TMAZ. In turn, coarsened and coalesced particles were observed in the HAZ. The use of post-weld direct tempering (PWDT) resulted in the reprecipitation of particles in SZ and TMAZ, and in the case of a lower rotational speed (200RPM), these particles had a more homogeneous character. In general, the authors recommend welding at low rotational speeds so that the temperature generated remains below the tempering temperature employed for base material (BM).

In turn, in [68] the transformations of precipitations in AISI 317L steel were analyzed in three stages: base material, immediately after FSW and after thermal aging at 550°C for up to about 400 hours. No intermetallic phases were observed immediately after welding. However, fine intermetallic precipitates uniformly distributed in the ferrite islands appeared in aged specimens. With increasing aging time and development of precipitation phenomena, the content of ferrite gradually decreased. Intermetallic precipitates formed Cr and Mo rich phases precursor to sigma phase.

A separate problem is the phase analysis of dissimilar joints. In one of the papers devoted to this issue [69], the joint of RAFM and 316L steel was analyzed. Ni diffusion from 316L to RAFM steel was observed in SZ. Excess of Ni in RAFM resulted in the formation of a dual-phase structure consisting of martensite/ferrite and austenite adjoining the bonding interface. Interestingly, it was found that from the point of view of the quality and strength of the joint, it was more advantageous to place 316L steel on the advancing side.

5.3. Aluminum alloys

Due to the widespread use of the FSW technology in the welding of aluminum alloys, a relatively large amount of work has been devoted to the problem of precipitation phenomena in this type of materials.

For example, Ma et al. [70] compared the microstructure of as cast A356 aluminum alloy and the same materials after FSP. A complex structure with needle-shaped Si particles, primary aluminum dendrites and voids/pores was observed in the as cast material (Fig. 5a).

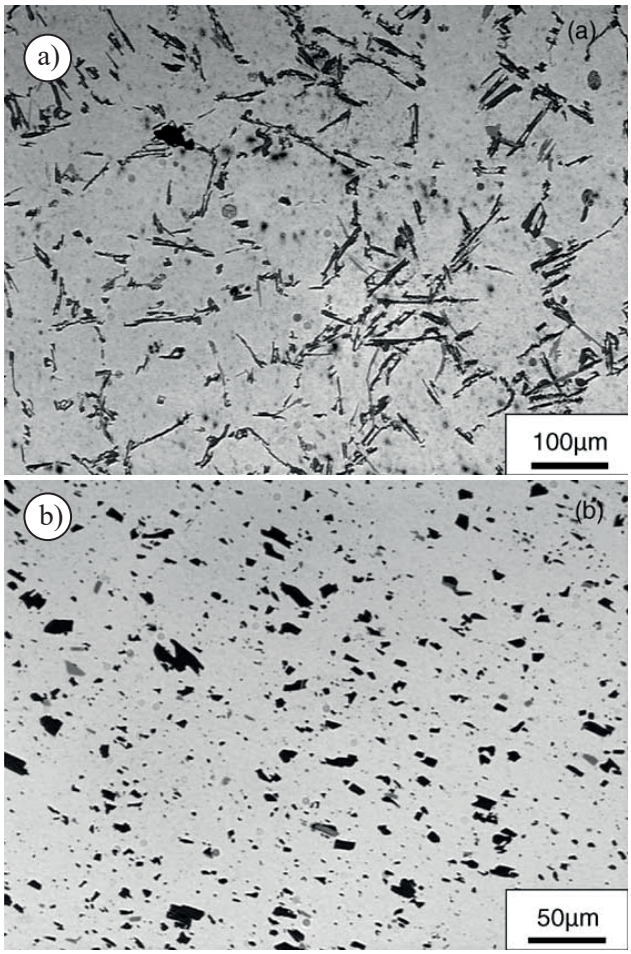

Fig. 5. Microstructure of A356 as cast aluminum alloy: a) microstructure of A356 as cast aluminum alloy, b) microstructure after FSW [4, 70]

The base material was then subjected to FSP at the tool rotation speed of 900RPM and a travel speed of 203 mm/min. As a result, the structure visible in Figure 5b was obtained. FSP resulted in the fragmentation of Si particles, aluminum dendrites and their uniform distribution in the material volume. In addition, a reduction in the material porosity was observed.

In [71], the distribution of precipitates in the cross section of the FSW joint was analyzed. Two types of the 7449 aluminum alloy ageing conditions were taken into account, namely: T3 (naturally aged) and T79 (over-aged). Plates with a thickness of 6.5 mm were welded at a constant tool rotational speed of 350RPM and at two linear speeds: 175 mm/min (low speed) and 350 mm/min (high speed). In the next stage, the structure of individual weld areas was examined using optical microscopy, transmission electron microscopy (TEM) and, above all, small-angle X-ray scattering (SAXS).

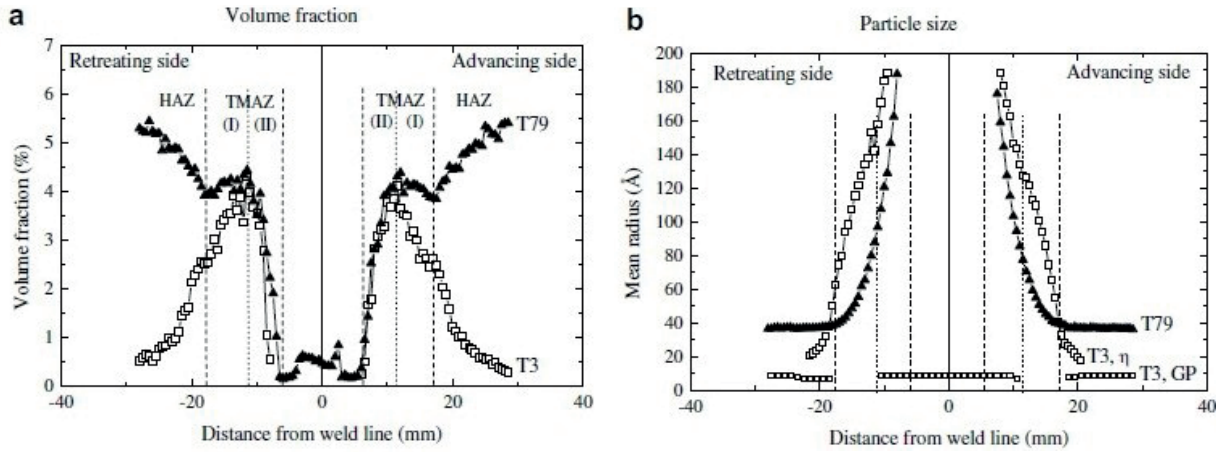

Fig. 6. Basic geometrical characteristics of precipitations in the FSW joint cross section for 7449 aluminum alloys in T3 (naturally aged) and T79 (over-aged) states: a) volume fraction; b) mean particle size [71]

In Figure 6 the volume fraction and mean particle size, obtained with SAXS, are presented. In terms of the analyzed parameters, no significant differences between retreating and advancing side were observed. However, the large difference in precipitates volume fraction between the T3 and T79 materials can be found. In the case of the T79 alloy, a rapid decrease in the precipitations fraction is observed in the HAZ, which is associated with the impact of heat and the accompanying dissolution of parent material hardening precipitates. As can be seen from Figure 6b, these processes were not accompanied by a significant change in particle size.

On the other hand, in TMAZ, on the HAZ side, a slight increase in the fraction of particles is observed, followed by a sharp decrease, to about 0%, close to SZ. A characteristic feature of TMAZ is also a constant increase in particle size with decreasing distance to SZ.

Precipitates in the SZ and TMAZ of the T3 alloy joints have similar characteristics. However, in HAZ, the weld showed a completely different behavior than before. With decreasing distance to the TMAZ, the volume fraction of particles increased rapidly. Their constant size, similar to the parent material, suggests the nucleation of new particles.

The analysis of the microstructure of FSW joints of aluminum 2024 T351 and 2024 T6 alloys, both in terms of grain structure changes and hardening precipitates, is discussed in detail in [72]. In the case of 2024 T351 alloy base material, all precipitations had the form of Guinier Preston Bagaryatskii (GPB) zones (age hardening with fully coherent metastable precipitates [73]). In HAZ, under the influence of temperature, GPBs dissolved and then were replaced by S'(S) (Al_2CuMg) precipitates. Susequently, the precipitates grew, which led to a decrease in the hardness of the material at the HAZ/TMAZ border. A similar phenomenon occurred in TMAZ. On the other hand, in nugget, high temperature resulted in a small number of coarse S'(S) phase, while a large amount of solute enabled nucleation of GPB zones.

Similar phenomena occurred in 2024 T6 alloy, although in the HAZ area, in the vicinity of the base material, the S'(S) particles were characterized by smaller sizes, which directly translated into a slightly higher hardness than in the case of 2024 T351 alloy.

The aforementioned decrease in the hardness of the 2024 T351 alloy in HAZ was also observed in [74]. The authors, however, compared the properties of welds made by the traditional FSW method and those made by impulse friction stir welding (IFSW). The characteristic feature of IFSW is the additional, vertical movement of the tool, which causes a sinusoidal change in the vertical force. In the case of IFSW joints, a higher hardness in the HAZ zone was observed than in the case of FSW. The authors [74] attribute this phenomenon to additional deformations caused by mechanical impulses, which in combination with the influence of temperature promoted reprecipitation of fine S particles at the dislocations and low angle grain boundaries. The presence of fine S particles had a positive effect on the strength of the material in HAZ.

A detailed analysis of the microstructural changes of both alloys (2024 T351 and 2024 T6) during friction surfacing (FS) was also conducted in [75]. In this case, FS involved the deposition of AA2024 T6 coating with the friction method on a substrate in the form of a sheet of AA2024 T351 aluminum alloy. A detailed analysis of temperature changes and associated phase transitions

in the HAZ was carried out using DSC (differential scanning calorimetry), TEM and SAXS techniques. The theoretical description of phase transformations in 2024 alloy, according to [76], was compared with the results of heat flux assessed by DSC. This allowed the estimation of changes in the microstructure during FS, depending on the range of process temperatures. Between 160°C and 210°C dissolution of GP(I)/GPB zones and θ”/S” phase was observed. In the next stage, exothermic transformations occurring in the range of 250-300°C were assigned to the precipitation of θ’/S’ phase. Between 300°C and 470°C θ’/S’ phases dissolved or transformed into a stable θ (Al_2Cu)/S (Al_2CuMg) phase.

The occurrence of microstructural changes including precipitates dissolution and reprecipitation depends on both the material chemical composition and the temperature related to the type of tool used and technological parameters. For example, in [77], microstructural changes of aluminum alloys Al-Mg-Si (6061 AA) and Al-Mg-Sc were compared. In the case of the first alloy, the rotational speed of the tool was 400RPM and travel speed was 2 mm/s. The analogous values for the second alloy were 500RPM and 1 mm/s. With similar welding parameters, different nugget zone microstructures were obtained. In the case of the Al-Mg-Si alloy, almost complete dissolution of the β” phase was observed, which in turn resulted in a significant decrease in the hardness in the nugget zone. The ageing treatment allowed reprecipitation to some extent and improved material properties.

In turn, in the case of the Al-Mg-Sc alloy, no dissolution or coarsening of the Al_3Sc strengthening phase was observed. The decrease in hardness of the material compared to the parent material was therefore small. It was also found that the Al_3Sc particles interacted with the boundaries of recrystallized grains, which in turn limited grain growth. Microstructural studies showed the presence of both coherent and incoherent Al_3Sc particles in the nugget zone.

In the work [65], the microstructure and mechanical properties of 2219Al T6 aluminum alloy joints were compared for different rotational and linear speeds of the tool. The joint properties depended on the Al_2Cu phase transitions. The growth of these particles was dependent on the overaging time (duration above the aging temperature of 190°C), which in turn was dependent on the linear speed and was independent on the rotational speed. Increasing the linear speed from 100 mm/min to 400 mm/min shortened the overaging time, limited particle growth, and consequently increased hardness and strength in the low hardness zone (LHZ). However, a further increase in the linear welding speed (up to 800 mm/min) did not result in an increase in these parameters.

The analysis of phase transformations during FSW can also be carried out by numerical analysis or a methodology combining experimental research and finite element method (FEM) simulation. For example, in [78], a multi-stage microstructural analysis of joints of aluminum alloys 2017A-T451 and 7075-T651 was performed. Using the DSC technique, changes in the heat flux in the weld were determined, which allowed the detection of areas of phase transitions in the welded material. Then, the results obtained in this way were included into the computational model [15], which enabled the numerical determination of maps of phase transformations occurring in the material during welding. It was shown that the temperature generated near the weld center was sufficient to completely dissolve the equilibrium η phase in 7075-T651 alloy and partially dissolve the equilibrium S phase in 2017A-T451 alloy. Gradual cooling of the weld led to Guinier-Preston (GP) and Guinier-Preston-Bagaryatskii (GPB) zones reprecipitation, which led to an increase in the material hardness.

The obtained results were subjected to indirect verification, based on the measurement of hardness changes in individual areas of the weld and positron lifetime curves across the weld. Changes in both of these parameters turned out to be well correlated with the phase transitions predicted in the numerical model.

Another technique that enables the study and description of changes in the microstructure of the material during FSW is the measurement of the electrical conductivity of individual areas of the weld. An example of using this technique to test joints of aluminum alloys AA 7075 T6 and AlMgSc is described in [79]. However, it was indicated that in the case of the tested alloys, the change in conductivity is primarily the result of the grain size, and is not dependent on the presence of precipitates. Therefore, their assessment is difficult.

As mentioned in the previous section, the use of the bobbin tool (BT) results in high welding temperatures and poor heat dissipation. Therefore, dissolution and coarsening of second phase particles is more intense, which is not favorable from the point of view of weld strength, especially in the case of high rotational speeds of the tool [80]. These disadvantages can be reduced to some extent by spraying/water cooling the workpieces [81] or postweld heat treatment.

6. CONCLUSIONS

FSW, despite its relatively short history, turned out to be an excellent tool for joining metal alloys used in industry (primarily aluminum). The great success of this technology is evidenced by a wide range of applications, a huge number of scientific publications on it (also in recent years), as well as numerous derivative technologies (such as FSP/FSA).

Although a significant number of studies and publications have been devoted to the properties of FSW joints, there are still many unexplored issues regarding the impact of technological parameters on the microstructure of welds. Since microstructural changes greatly affect the strength properties, understanding them is crucial to ensuring the safety of the structure.

In general, the structure of individual weld areas depends on the temperature, which is influenced by the type of welded material, the tool and technological parameters (mainly rotational speed and travel speed).

The history of plastic deformation and heating/cooling conditions determine the course of grain recrystallization, which is particularly intense in SZ. As a result of these changes, the grains are refined, which directly affects the improvement of mechanical properties in this zone.

As described above, several recrystallization mechanisms are possible, which depend on the crystal structure of the base material and its stacking fault energy (SFA).

The second factor determining the properties of the weld, especially in particle strengthened aluminum alloys, are precipitation phenomena, which in turn depend on thermal history. In areas with relatively low temperatures, existing particles coarsen or transform into more stable phases. On the other hand, in areas with higher temperatures (primarily SZ), the particles partially or completely dissolve. Depending on the cooling rate, the resulting solute may form new precipitates. Since the material contains the crystal structure defects, which are sites of reprecipitation, the formation of these particles is heterogeneous.

REFERENCES

[1] Yang Y., Bi J., Liu H., Li Y., Li M., Ao S., Luo Z.: *Research progress on the microstructure and mechanical properties of friction stir welded Al–Li alloy joints*, Journal of Manufacturing Processes, 82 (2022), 230-244.
[2] Lambiase F., Derazkola H.A., Simchi A.: *Friction stir welding and friction spot stir welding processes of polymers-state of the art*, Materials, 13 (2020), 2291.
[3] Çam G., Javaheri V., Heidarzadeh A.: *Advances in FSW and FSSW of dissimilar Al-alloy plates*, Journal of Adhesion Science and Technology, 37(2) (2023), 162-194.
[4] Mishra R.S., Ma Z.Y.: *Friction stir welding and processing*, Materials Science and Engineering: R: Reports, 50 (2005), 1-78.
[5] He X., Gu F., Ball A.: *A review of numerical analysis of friction stir welding*, Progress in Materials Science, 65 (2014), 1-66.
[6] Li K., Liu X., Zhao Y.: *Research status and prospect of friction stir processing technology*, Coatings, 9(2) (2019), 129.
[7] Rhodes C.G., Mahoney M.W., Bingel W.H., Spurling R.A., Bampton C.C.: *Effects of friction stir welding on microstructure of 7075 aluminum*, Scripta Materialia, 36 (1997), 69-75.
[8] Morisada Y., Fujii H., Nagaoka T., Nogi K., Fukusumi M.: *Fullerene/A5083 composites fabricated by material flow during friction stir processing*, Composites Part A, 38 (2007), 2097-2101.
[9] Meng X., Huang Y., Cao J., Shen J., dos Santos J.F.: *Recent progress on control strategies for inherent issues in friction stir welding*, Progress in Materials Science, 115 (2021), 100706.
[10] Jemioło S., Gajewski M.: *Symulacja MES obróbki cieplnej wyrobów stalowych z uwzględnieniem zjawisk termo-metalurgicznych*, Część 1. Nieustalony przepływ ciepła z uwzględnieniem przejść fazowych, Zeszyty Naukowe, Budownictwo, z. 143, Oficyna Wydawnicza PW, Warszawa 2005.
[11] Jemioło S., Gajewski M.: *Symulacja MES obróbki cieplnej wyrobów stalowych z uwzględnieniem zjawisk termo-metalurgicznych*, Część 2. Przykłady numeryczne z zastosowaniem programu SYSWELD, Zeszyty Naukowe, Budownictwo, z. 143, Oficyna Wydawnicza PW, Warszawa 2005.
[12] Jemioło S., Gajewski M.: *Zastosowanie programu SYSWELD w modelowaniu resztkowych naprężeń pospawalniczych*, Zeszyty Naukowe, Budownictwo, z. 143, Oficyna Wydawnicza PW, Warszawa 2005.
[13] Kossakowski P.G., Wciślik W., Bakalarz M.: E*ffect of selected friction stir welding parameters on mechanical properties of joints*, Archives of Civil Engineering, 65(4) (2019), 51-62.
[14] Jacquin D., Guillemot G.: *A review of microstructural changes occurring during FSW in aluminium alloys and their model-ling*, Journal of Materials Processing Technology, 288 (2021), 116706.

[15] Hamilton C., Dymek S., Dryzek E., Kopyściański M., Pietras A., Węglowska A., Wróbel M.: *Application of positron lifetime annihilation spectroscopy for characterization of friction stir welded dissimilar aluminum alloys*, Materials Characterization, 132 (2017), 431-436.
[16] Patel V., Li W., Vairis A., Badheka V.: *Recent development in friction stir processing as a solid-state grain refinement technique: microstructural evolution and property enhancement*, Critical Reviews in Solid State and Materials Sciences, 5 (2019), 378-426.
[17] Reynolds A.P.: *Visualisation of material flow in autogenous friction stir welds*, Science and Technology of Welding and Joining, 5(2) (2000), 120-124;
[18] Seidel T.U., Reynolds A.P.: *Visualization of the material flow in AA2195 friction-stir welds using a marker insert technique*, Metallurgical and Materials Transactions A, 32 (2001), 2879-2884.
[19] Colligan K.: *Material flow behavior during friction stir welding of aluminum*, Welding Journal, 78 (1999), 229-s-237-s.
[20] Schmidt H.N.B., Dickerson T.L., Hattel J.H.: *Material flow in butt friction stir welds in AA2024-T3*, Acta Materialia, 54 (2006), 1199-209.
[21] Ouyang J.H., Kovacevic R.: *Material flow and microstructure in the friction stir butt welds of the same and dissimilar aluminum alloys*, Journal of Materials Science, 11 (2002), 51-63.
[22] Li Y., Murr L.E., McClure J.C.: *Solid-state flow visualization in the friction-stir welding of 2024 Al to 6061 Al*, Scripta Materialia, 40(9) 1999, 1041-1046.
[23] Colegrove P.A., Shercliff H.R.: *3-Dimensional CFD modelling of flow round a threaded friction stir welding tool profile*, Journal of Materials Science, 169 (2005), 320-327.
[24] Nandan R., DebRoy T., Bhadeshia H.K.D.H.: *Recent advances in friction-stir welding – Process*, weldment structure and properties, Progress in Materials Science, 53 (2008), 980-1023.
[25] El-Sayed M.M., Shash A.Y., Mahmoud T.S., Abd-Rabbou M.: *Effect of friction stir welding parameters on the peak tem-perature and the mechanical properties of aluminum alloy 5083-O*, Advanced Structured Materials, 72 (2018), 11-25.
[26] El-Sayed M.M., Shash A.Y., Abd-Rabou M., ElSherbiny M.G.: *Welding and processing of metallic materials by using friction stir technique: A review*, Journal of Advanced Joining Processes, 3 (2021), 100059.
[27] Cho J.H., Boyce D.E., Dawson P.R.: *Modeling strain hardening and texture evolution in friction stir welding of stainless steel*, Materials Science and Engineering: A, 398 (2005), 146-163.
[28] Ma Z.Y.: *Friction stir processing technology: A review, Metallurgical and Materials Transactions A*, 39 (2008), 642-658.
[29] Prakash P., Jha S.K., Lal S.P.: *Numerical investigation of stirred zone shape and its effect on mechanical properties in friction stir welding process*, Welding World, 63 (2019), 1531-1546.
[30] Chen K., Liu X., Ni J.: *A review of friction stir–based processes for joining dissimilar materials*, The International Journal of Advanced Manufacturing Technology, 104 (2019), 1709-1731.
[31] Gallais C., Denquin A., Bréchet Y., Lapasset G.: *Precipitation microstructures in an AA6056 aluminium alloy after friction stir welding: characterisation and modelling*, Materials Science and Engineering: A, 496 (2008), 77-89.
[32] Hattel J.H., Schmidt H.N.B., Tutum C.: *Thermomechanical modelling of friction stir welding.* The 8th International Conference Trends in Welding Research, Pine Mountain, Georgia, USA, 2008.
[33] Imam M., Biswas K., Racherla V.: *On use of weld zone temperatures for online monitoring of weld quality in friction stir welding of naturally aged aluminium alloys*, Materials & Design, 52 (2013), 730-739.
[34] Jacquin D., De Meester B., Simar A., Deloison D., Montheillet F., Desrayaud C.: *A simple Eulerian thermomechanical modelling of friction stir welding*, Journal of Materials Processing Technology, 211(1) (2011), 57-65.
[35] Tang W., Guo X., McClure J.C., Murr L.E.: *Heat input and temperature distribution in friction stir welding*, Journal of Materials Processing and Manufacturing Science, 7(2) (1998), 163-172.
[36] Sharma V., Prakash U., Kumar B.V.M.: *Surface composites by friction stir processing: A review*, Journal of Materials Processing Technology, 224 (2015), 117-134.
[37] Rodrigues D.M., Loureiro A., Leitao C., Leal R.M., Chaparro B.M., Vilaça P.: *Influence of friction stir welding parameters on the microstructural and mechanical properties of AA 6016-T4 thin welds*, Materials & Design, 30 (2009), 1913-1921.
[38] Węglowski M.S.: *Friction stir processing – State of the art*, Archives of Civil and Mechanical Engineering, 18 (2018), 114-129.
[39] Givi M.K.B., Asadi P.: *Advances in friction stir welding and processing*. Woodhead Publishing, Amsterdam, 2014.
[40] Kassner M.E., Barrabes S.: *New developments in geometric dynamic recrystallization*, Materials Science and Engineering: A, 410 (2005), 152-155.

[41] Heidarzadeh A., Mironov S., Kaibyshev R., Çam G., Simar A., Gerlich A., Khodabakhshi F., Mostafaei A., Field D.P., Robson J.D., Deschamps A., Withers P.J.: *Friction stir welding/processing of metals and alloys: A comprehensive review on microstructural evolution*, Progress in Materials Science, 117 (2021), 100752.
[42] Dudova N., Belyakov A., Sakai T., Kaibyshev R.: *Dynamic recrystallization mechanisms operating in a Ni–20% Cr alloy under hot-to-warm working*, Acta Materialia, 58 (2010), 3624-3632.
[43] Liu H., Fujii H.: *Microstructural and mechanical properties of a beta-type titanium alloy joint fabricated by friction stir welding*, Materials Science and Engineering: A, 711 (2018), 140-148.
[44] Humphreys F.J., Hatherly M.: *Recrystallization and related annealing phenomena*, Elsevier, 2004.
[45] Prabhu S.R.B., Shettigar A.K., Herbet M.A., Rao S.S.: *Microstructure evolution and mechanical properties of friction stir welded AA6061/Rutile composite*, Materials Research Express, 6(8) (2019), 0865i7.
[46] Padmanaban G., Balasubramanian V., Sarin Sundar J.K.: *Influences of welding processes on microstructure, hardness, and tensile properties of AZ31B magnesium alloy*, Journal of Materials Engineering and Performance, 19 (2010), 155-165.
[47] Wciślik W.: *Experimental determination of critical void volume fraction f_F for the Gurson Tvergaard Needleman (GTN) model*, Procedia Structural Integrity, 2 (2016), 1676-1683.
[48] Wciślik W., Pała R.: *Some microstructural aspects of ductile fracture of metals*, Materials, 14(15) (2021), 4321.
[49] Wciślik W., Lipiec S.: *Void-induced ductile fracture of metals: experimental observations*, Materials, 15(18) (2022), 6473.
[50] Dixit S., Mahata A., Mahapatra D.R., Kailas S.V., Chattopadhyay K.: *Multi-layer graphene reinforced aluminum – Manufacturing of high strength composite by friction stir alloying*, Composites Part B: Engineering, (136) (2018), 63-71.
[51] Merah N., Azeem M.A., Abubaker H.M., Al-Badour F., Albinmousa J., Sorour A.A.: *Friction stir processing influence on microstructure, mechanical, and corrosion behavior of steels: a review*, Materials, (14) (2021), 5023.
[52] Sato Y.S., Nelson T.W., Sterling C.J., Steel R.J., Pettersson C.O.: *Microstructure and mechanical properties of friction stir welded SAF 2507 super duplex stainless steel*, Materials Science and Engineering: A, (397) (2005), 376-384.
[53] Kwon Y.J., Saito N., Shigematsu I.: *Friction stir process as a new manufacturing technique of ultrafine grained aluminium alloy*, Journal of Materials Science, (21) (2002), 1473-1476.
[54] Saeid T., Abdollah-zadeh A., Assadi H., Malek Ghaini F.: *Effect of friction stir welding speed on the microstructure and mechanical properties of a duplex stainless steel*, Materials Science and Engineering: A, (496) (2008), 262-268.
[55] Ma Z.Y., Mishra R.S., Mahoney M.W.: *Superplastic deformation behaviour of friction stir processed 7075Al alloy*, Acta Materialia, 50(17) (2002), 4419-4430.
[56] Johnson P., Murugan N.: *Microstructure and mechanical properties of friction stir welded AISI321 stainless steel*, Journal of Materials Research and Technology, 9(3) (2020), 3967-3976.
[57] Gain S., Das S.K., Sanyal D., Acharyya S.K.: *Exploring friction stir welding for joining 316L steel pipes for industrial applications: Mechanical and metallurgical characterization of the joint and analysis of failure*, Engineering Failure Analysis, 150 (2023), 107331.
[58] Li H., Yang S., Zhang S., Zhang B., Jiang Z., Feng H., Han P., Li J.: *Microstructure evolution and mechanical properties of friction stir welding super-austenitic stainless steel S32654*, Materials and Design, 118 (2017), 207-217.
[59] Ahmed M.M.Z., Hajlaoui K., El-Sayed Seleman M.M., Elkady M.F., Ataya S., Latief F.H., Habba M.I.A.: *Microstructure and mechanical properties of friction stir welded 2205 duplex stainless steel butt joints*, Materials, 14 (2021), 6640.
[60] Liu F.C., Nelson T.W.: *In-situ grain structure and texture evolution during friction stir welding of austenite stainless steel*, Materials and Design, 115 (2017), 467-478.
[61] Salih O.S., Ou H., Sun W., McCartney D.G.: *A review of friction stir welding of aluminium matrix composites*, Materials & Design, (86) (2015), 61-71.
[62] Zhang Z., Xiao B.L., Ma Z.Y.: *Effect of welding parameters on microstructure and mechanical properties of friction stir welded 2219Al-T6 joints*, Journal of Materials Science, (47) (2012), 4075-4086.
[63] Huang K., Marthinsen K., Zhao Q., Logé R.E.: *The double-edge effect of second-phase particles on the recrystallization behaviour and associated mechanical properties of metallic materials*, Progress in Materials Science, (92) (2018), 284-359.
[64] Kloc L., Spigarelli S., Cerri E., Evangelista E., Langdon T.G.: *Creep behavior of an aluminum 2024 alloy produced by powder metallurgy*, Acta Materialia, (45) (1997), 529-540.
[65] Deschamps A., Fribourg G., Bréchet Y., Chemin J.L., Hutchinson C.R.: *In situ evaluation of dynamic precipitation during plastic straining of an Al-Zn-Mg-Cu alloy*, Acta Materialia, (60) (2012), 1905-1916.

[66] Sugimoto I., Park S.H.C., Hirano S., Saito H., Hata S.: *Microscopic observation of precipitation behavior at friction stirring zone of super duplex stainless steel*, Materials Transactions, 60(9) (2019), 2003-2007.
[67] Manugula V.L., Rajulapati K.V., Reddy G.M., Mythili R., Bhanu Sankara Rao K.: *Influence of tool rotational speed and post-weld heat treatments on friction stir welded reduced activation ferritic-martensitic steel*, Metallurgical and Materials Transactions A: Physical Metallurgy and Materials Science, 48(8) (2017), 3702-3720.
[68] Farneze H.N., Tavares S.S.M., Pardal J.M., Londoño A.J.R., Pereira V.F., Barbosa C.: *Effects of thermal aging on microstructure and corrosion resistance of AISI 317L steel weld metal in the FSW process*, Materials Research, 18(2) (2015), 98-103.
[69] He B., Cui L., Wang D.P., Li H.J., Liu C.X.: *Microstructure and mechanical properties of RAFM-316L dissimilar joints by friction stir welding with different butt joining modes*, Acta Metallurgica Sinica (English Letters), 33 (2020), 135-146.
[70] Ma Z.Y., Sharma S.R., Mishra R.S., Mahoney M.W.: Unpublished results.
[71] Dumont M., Steuwer A., Deschamps A., Peel M., Withers P.J.: *Microstructure mapping in friction stir welds of 7449 alu-minium alloy using SAXS*, Acta Materialia, (54) (2006), 4793-4801.
[72] Genevois C., Deschamps A., Denquin A., Doisneau-Cottignies B.: *Quantitative investigation of precipitation and mechanical behaviour for AA2024 friction stir welds, Acta Materialia*, (53) (2005), 2447-2458.
[73] Bastow T.J., Hill A.: *Guinier-Preston and Guinier-Preston-Bagaryatsky zone reversion in Al-Cu-Mg alloys studied by NMR*, Materials Science Forum, (519-521) (2006), 1385-1390.
[74] Morozova I., Królicka A., Obrosov A., Yang Y., Doynov N., Weiß S., Michailov V.: *Precipitation phenomena in impulse friction stir welded 2024 aluminium alloy*, Materials Science and Engineering A, (852) (2022), 143617.
[75] Ehrich J., Staron P., Karkar A., Roos A., Hanke S.: *Precipitation evolution in the heat-affected zone and coating material of AA2024 processed by friction surfacing*, Advanced Engineering Materials, (24) (2022), 2201019.
[76] Ostermann F.: *Anwendungstechnologie aluminium*. Springer-Verlag, Berlin, 2014.
[77] Sauvage X., Dédé A., Cabello Muñoz A., Huneau B.: *Precipitate stability and recrystallisation in the weld nuggets of friction stir welded Al-Mg-Si and Al-Mg-Sc alloys*, Materials Science and Engineering A, (491) (2008), 364-371.
[78] Hamilton C., Dymek S., Kopyściański M., Węglowska A., Pietras A.: *Numerically based phase transformation maps for dissimilar aluminum alloys joined by friction stir-welding*, Metals, 8(5) (2018), 324.
[79] Santos T.G., Miranda R.M., Vilaça P., Teixeira J.P., dos Santos J.: *Microstructural mapping of friction stir welded AA 7075-T6 and AlMgSc alloys using electrical conductivity*, Science and Technology of Welding and Joining, 16(7) (2011), 630-635.
[80] Hou J.C., Liu H.J., Zhao Y.Q.: *Influences of rotation speed on microstructures and mechanical properties of 6061–T6 aluminum alloy joints fabricated by selfreacting friction stir welding tool*, International Journal of Advanced Manufacturing Technology, (73) (2014), 1073-1079.
[81] Zhao Y., Wang C., Dong C.: *Microstructural characteristics and mechanical properties of water cooling bobbin-tool friction stir welded 6063-T6 aluminum*, MATEC Web of Conferences, (206) (2018), 03002.